ACS APPLIED MATERIALS & INTERFACES

www.acsami.org

Research Article

The Role of the Hydrogen Bond between Piperazine and Fullerene Molecules in Stabilizing Polymer:Fullerene Solar Cell Performance

Zerui Li, Jiankai Shan, Lingpeng Yan, Huimin Gu, Yi Lin, Hongwei Tan,* and Chang-Qi Ma*

Cite This: *ACS Appl. Mater. Interfaces* 2020, 12, 15472−15481

Read Online

ACCESS | Metrics & More | Article Recommendations | Supporting Information

ABSTRACT: Piperazine has been recently reported as a stabilizer for polymer:fullerene solar cells that can minimize the "burn-in" degradation of the cell. In this paper, the influence of N-substituents on the stabilization effect of piperazine in P3HT:$PC_{61}BM$ cells was investigated. Results confirmed that only piperazine derivatives (PZs) with N−H bonds showed the stabilization effect, whereas the bis-alkyl-substituted piperazine compounds cannot improve the stability. An efficient photon-induced electron transfer (PET) process between PZ and $PC_{61}BM$ was only detected for the N−H-containing PZ:$PC_{61}BM$ blends, corresponding very well to the stabilization effect of the PZs, which indicates that the PET process between PZ and $PC_{61}BM$ stabilizes the cell performance, and the N−H bond plays a critical role ensuring the PET process and the consequent stabilization effect. Both ^{1}H-NMR spectroscopy and theoretical calculations confirmed the formation of N−H···O−C and N−H···π bonds for the $PC_{61}BM$:piperazine adduct, which was considered as the driving force that promotes the PET process between these two components. In addition, comparison of the calculated electron affinity energy (E_A) and excitation energy (E_{Ex}) of $PC_{61}BM$ with/without piperazine confirmed that piperazine doping is able to promote the electron transfer (which leads to the formation of $PC_{61}BM$ anions) than the energy transfer (leads to the formation of $PC_{61}BM$ excitons) between P3HT and $PC_{61}BM$, which is beneficial for the performance and stability improvement.

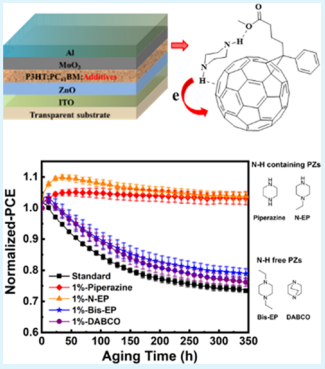

KEYWORDS: *Polymer Solar Cells, Photochemistry, Degradation and Stability, Piperazine, Hydrogen Bond*

1. INTRODUCTION

Polymer solar cells (PSCs) are considered as the next-generation photovoltaic technology because of their advantages of low cost,[1] excellent flexibility,[2,3] lightweight,[4] ease of large-area fabrication,[5] and low-toxicity properties.[6] In the past two decades, numerous studies have been done in improving the power conversion efficiencies (PCEs) of PSCs, and now, the highest PCE has reached over 16% in single junction devices[7,8] and 17% in tandem cells,[9] getting closer to that of traditional silicon solar cells. With the great achievement of high PCEs, the limit to the application of PSCs turns to be the relatively poor stability.[6,10,11]

More and more efforts have been devoted to investigating the decay mechanism of polymer solar cells and to lengthening their lifetime.[12−14] Various degradation pathways have been clearly clarified recently, such as photon-induced oxidation of conjugated molecules,[13,15] oxidation of electrodes,[16] nanomorphology changes owing to the thermal molecular motions,[17] and electric-field-induced molecule redistributions.[18] Among which, performance decays caused by moisture and/or oxygen erosion are considered as extrinsic decay processes,[19] which can be effectively suppressed by proper encapsulation. In contrast, performance decays that originated from molecular rearrangement or crystallization by thermal heating[17] or electronic filed polarizing,[18] or fullerene molecule dimerization by light illumination,[20] are intrinsic decay processes,[21] which cannot be simply suppressed by encapsulation. The intrinsic decay processes determine the potential longest lifetime of PSCs, and are considered as the most important issue for the degradation study in PSCs.

The recent research results demonstrated that fast "burn-in" degradations[19,22] are found in most of the polymer solar cells, which generally led to 30−50% PCE loss at the first hundred hours.[19] Understanding the degradation mechanism of the intrinsic burn-in decay process and finding a method to suppress the burn-in process are of great interest since this will dramatically improve the lifetime and power output of the solar cells. Doping a third compound in the photoactive layer is considered to be the simplest way to improve device stability. For example, Turkovic et al. and Brabec et al. reported the use of chemical additives to suppress the formation of radicals in the polymer blends, and consequently improve the device stability.[23−25] For polymer:fullerene solar cells, dimerization of fullerene molecules under light illumination was found to be the main reason for the burn-in decay.[20,26,27] By systematically

Received: December 30, 2019
Accepted: March 6, 2020
Published: March 6, 2020

investigating the external load dependence of the decay process, we have recently confirmed that the fast J_{SC} decay in polymer P3HT:$PC_{61}BM$ cells is related to the concentration of fullerene excitons.[27] Based on this finding, we established an effective method of doping the photoactive layer with piperazine to minimize the burn-in decay of the P3HT:$PC_{61}BM$ cells.[27,28] Interestingly, we also found that piperazine doping can increase the device performance. The simultaneous enhancement of performance and stability was ascribed to the effective quenching of the fullerene triplet by piperazine, which minimizes the dimerization of $PC_{61}BM$ and enhances the electron density within the $PC_{61}BM$ domain.[28] Following this, Brabec et al. also demonstrated that piperazine doping is able to improve device stability of PCE11:$PC_{71}BM$ cells,[29] demonstrating the generality of the piperazine doping effect. To further understand the detailed working mechanism on the performance and stability improvement of piperazine doping and to find more potential stabilizers for use in polymer solar cells, in this paper, we systematically investigate the stabilization effect of N-substituents of piperazines (PZs). Results confirmed that only compounds having N−H bonds show a positive stabilization effect in polymer:fullerene solar cells. The ^{1}H-NMR analyses and theoretical calculations confirmed that H-bonds formed between PZs and fullerene molecules through N−H···O−C and N−H···π bonding, which brings them closer and consequently ensures efficient photon-induced electron transfer between piperazine and fullerene molecules. In addition, the electron affinity energy (E_A) and excitation energy (E_{Ex}) for $PC_{61}BM$ were calculated to be lowered by 3.48 and 0.35 kcal/mol after doping with piperazine, suggesting that piperazine would promote the photon-induced electron transfer (PET) than the photon-induced energy transfer (PEnT) between P3HT and $PC_{61}BM$, which is considered to be another important reason for the stability improvement of the piperazine additive.

2. EXPERIMENTAL SECTION

2.1. Materials. ITO substrates are custom-made on glass with a strip width of 3 or 4 mm. Regioregular poly(3-hexylthiophene-2,5-diyl) (P3HT, M_n = 5.0 × 10^4, PDI = 1.7, regioregularity rr = 95%) and [6,6]-phenyl-C_{61}-butyric acid methyl ester ($PC_{61}BM$) were purchased from Solarmer Energy, Inc. (Beijing) and Solenne B.V., respectively. Piperazine, *N*-ethylpiperazine (N-EP), *N*-aminoethylpiperazine (N-AEP), 1,4-bis(aminoethyl)piperazine (Bis-AEP), and 1-(2-aminoethyl)-4-methylpiperazine (M-AEP) were purchased from Adamas-Beta. 1,4-Bis(3-ethyl)piperazine (Bis-EP) was purchased from Alfa Aesar. Triethylenediamine (DABCO) was produced by Energy Chemical. Molybdenum(VI) oxide (MoO_3) was purchased from Strem Chemicals. Tetra-*n*-butylammonium hexafluorophosphate ($TBAPF_6$) was from J&K China Chemical Co. Ltd. All materials were used as received without further purification. ZnO nanoparticle solution was prepared through the reaction between KOH and $Zn(OAc)_2$ in methanol as reported by Beek et al.[30]

2.2. Instruments and Measurement. The ^{1}H-NMR spectra of piperazine with different weight ratios of $PC_{61}BM$ were measured with a Bruker Ascend (400 MHz) by adding $PC_{61}BM$ into a piperazine solution in benzene-d_6 (99.5 at. % D, J&K China, concentration of amine was 2 mg/mL). Cyclic voltammetry (CV) of $PC_{61}BM$ and PZs was carried out on an Autolab PGSTAT 302N. The sample concentration for the CV test was 10^{-3} mol/L in dry CH_2Cl_2. $TBAPF_6$ was used as the supporting electrolyte with a concentration of 0.1 mol/L. The reference electrode was Ag/Ag^+ (Ag^+ is from $AgNO_3$, 0.01 mol/L in CH_2Cl_2 with 0.1 mol/L $TBAPF_6$), and Fc/Fc^+ was used as the internal calibration standard (5 times the concentration of the sample). Electron spin resonance spectroscopy (ESR) of the $PC_{61}BM$ and $PC_{61}BM$:PZs films was carried out with an ESR spectrometer (Bruker E500). The sample for ESR measurement was prepared by putting a solution of $PC_{61}BM$ or $PC_{61}BM$:PZ in *ortho*-dichlorobenzene (ODCB, 200 μL, 20 mg/mL) into a standard 5 mm NMR tube, and the solvent was then removed under vacuum. The measurements were carried out at 90 K with or without light illumination from a xenon lamp (wavelength range from 200 to 800 nm).

2.3. Simulations and Quantum Chemistry Calculations. All theoretical calculations were carried out by using the Gaussian 09 program.[31] All the species were optimized by using the B3LYP density functional with the def2-SVP basis set.[32,33] Dispersion corrections were accounted for by using the D3 empirical formula by Grimme with Becke−Johnson damping.[34] BSSE corrections were considered in calculating the interaction energies.[35,36] The molecular radii were estimated by using Multiwfn.[37]

2.4. Fabrication of Organic Solar Cells. ITO substrates were sequentially cleaned by an ultrasonic bath in detergent, deionized water, acetone, and isopropanol and then were kept in isopropanol. The ITO substrates were first blow-dried by nitrogen gas flow and then treated in a UV-ozone oven for 30 min before use. First, filtered ZnO solution (12 mg/mL in methanol) was spin-coated on the ITO substrates at 2500 rpm for 60 s. Then the samples were annealed at 130 °C for 10 min on a hot plate. A solution of P3HT:$PC_{61}BM$ (20 mg/mL for each compound) blended with a certain amount of PZs (0.5, 1, 3, and 5%, weight of piperazine to total weight of P3HT and $PC_{61}BM$) in ODCB was stirred at 55 °C overnight before being spin-coated on the top of the ZnO electron transportation layer at 600 rpm for 60 s. The as-prepared P3HT:$PC_{61}BM$:PZs blend films were then put into a Petri dish with a cover and kept for 1.5 h to allow drying of the film slowly. Then the samples were annealed at 124 °C on a hot plate for 10 min. Finally, MoO_3 (20 nm) and Al (100 nm) were sequentially vacuum-deposited on the top of the active layer as the hole-extraction layer and the anode, respectively. The effective photovoltaic area, defined by the geometrical overlap between the bottom cathode electrode and the top anode, was 0.09 or 0.12 cm^2.

2.5. Performance Characterization of Organic Solar Cells. The performance of the devices was measured using a Keithley 2400 sourcemeter under illumination with simulated AM 1.5G sunlight (Verasol-2, LED 3A Sun simulator, Newport) in a nitrogen-filled glove box. The current density−voltage (J−V) curves were recorded, and open-circuit (V_{OC}), short-circuit current density (J_{SC}), fill factor (FF), and PCE were calculated accordingly by the home programmed software. The external quantum efficiency (EQE) spectra were recorded in a homebuilt EQE system where light from a 150 W tungsten halogen lamp (Osram 64610) was used as a probe light and was modulated with a mechanical chopper before passing through the monochromator (Zolix, Omni-k300) to select the wavelength. The response was recorded as the voltage by an I−V converter (D&R-IV Converter, Suzhou D&R Instruments) using a lock-in amplifier (Stanford Research Systems SR 830). A calibrated silicon cell was used as the reference before testing the devices. The device for EQE measurement was kept behind a quartz window in a nitrogen-filled container.

2.6. Degradation of Organic Solar Cell Performance under Illumination. The long-term stability of unencapsulated devices was conducted with a glove-box integrated multichannel solar cell performance decay test system (PVLT-G8001M, Suzhou D&R Instruments Co. Ltd.) under a testing condition in accordance with ISOS-L-1. The devices were put inside a nitrogen-filled glove box (H_2O < 3 ppm, O_2 < 3 ppm) and continuously illuminated with white LED light (D&R Light, L-W5300KA-150, Suzhou D&R Instruments). The illumination light intensity was initially set so that the output short-circuit current density (J_{SC}) equals that measured under standard conditions mentioned before and the photovoltaic devices work at their maximum power point (mpp). The illumination light intensity was monitored by a photodiode (Hamamatsu S1336-8BQ) to guarantee light intensity stability. J−V characteristics of the devices were checked periodically, and the photovoltaic performance data (V_{OC}, J_{SC}, FF, and PCE) were calculated automatically according to the J−V curves. After J−V sweeping, an external load that matches the

https://dx.doi.org/10.1021/acsami.9b23366
ACS Appl. Mater. Interfaces 2020, 12, 15472−15481

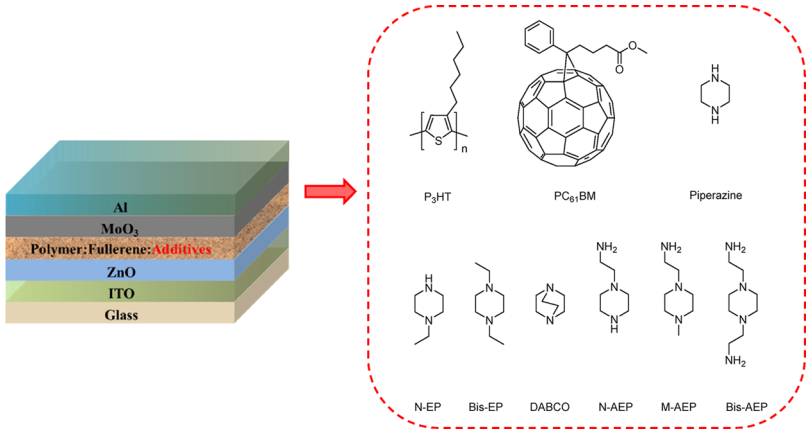

Figure 1. Device structure and molecule structures of active layer materials.

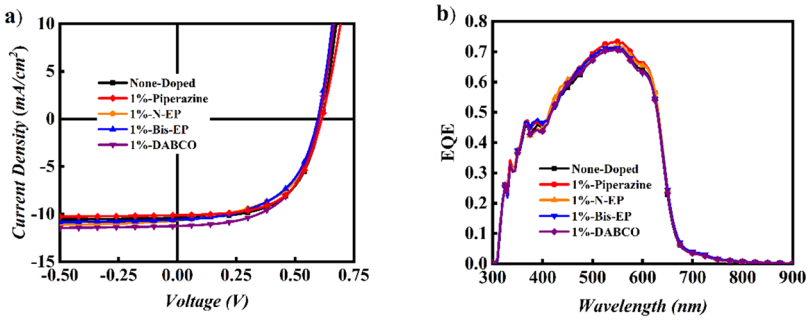

Figure 2. (a) $J-V$ and (b) EQE curves of P3HT: $PC_{61}BM$ cells doped with 1% piperazine, N-EP, Bis-EP, and DABCO.

Table 1. Performance of Devices Based on P3HT:$PC_{61}BM$ with 1% PZs

additive	V_{OC} (V)	J_{SC} (mA/cm^2)	FF	PCE (%)	T_{80} (h)[a]	η_{300}/η_0[b]
standard	0.60	10.34 ± 0.09	0.56 ± 0.01	3.57 ± 0.05	148	74%
piperazine	0.62	10.41 ± 0.19	0.57 ± 0.01	3.67 ± 0.09	≫300[c]	103%
N-EP	0.62	10.55 ± 0.13	0.54 ± 0.00	3.52 ± 0.04	≫300[c]	104%
Bis-EP	0.61	10.38 ± 0.12	0.57 ± 0.01	3.59 ± 0.03	281	80%
DABCO	0.60	10.49 ± 0.11	0.54 ± 0.01	3.40 ± 0.04	220	77%
N-AEP	0.60	10.28 ± 0.14	0.58 ± 0.01	3.55 ± 0.09	≫300[c]	100%
M-AEP	0.60	10.16 ± 0.06	0.57 ± 0.01	3.50 ± 0.07	≫300[c]	101%
Bis-AEP	0.60	10.37 ± 0.14	0.55 ± 0.01	3.46 ± 0.08	≫300[c]	102%

[a]Time that 80% of its initial PCE is reached. [b]η_0: PCE of the cell before aging, η_{300}: PCE of the cell after aging for 300 h. [c]Because the measuring time was limited to 300 h, the performance did not reach 80% of the initial PCE.

maximum power output point ($R_{mpp} = V_{max}/I_{max}$) was attached to the cell. So, the performance of devices under illumination can be recorded automatically over time, and the degradation curves were shown. Since external load changed according to the $J-V$ results, the measured performance decay curves imply the performance decay behavior of cells under real operation, fully meeting the load requirement for the highest level of ISOS-L-3. The cell temperature was measured occasionally, and the temperature range during aging was about 45−55 °C.

3. RESULTS AND DISCUSSION

3.1. Performance and Stability of PZs-Doped P3HT:$PC_{61}BM$ Cells. The sketch of organic solar cells and the structure of the material studied in this paper are shown in Figure 1. Our recent work demonstrated that mixing the P3HT:$PC_{61}BM$ blend film with a small amount of piperazine simultaneously improved device performance and stability, which was ascribed to the improvement of electron mobility of the blend film and the quenching of the $PC_{61}BM$ triplet by piperazine.[28] To better understand the influence of the molecular structure on the stabilizing effect in polymer solar cells, we fabricated and tested the performance and performance stability of P3HT:$PC_{61}BM$ cells doped with alkyl-chain-substituted PZs, including *N*-ethylpiperazine (N-EP), 1,4-bis(3-ethyl)piperazine (Bis-EP), and triethylenediamine (DABCO). Figure 2a,b depicts the representative $J-V$ curves and EQE spectra of the cells doped with 1.0% PZs, and the performance data are listed in Table 1. The complete photovoltaic performance characteristics including $J-V$ and EQE spectra of cells with weight doping ratios of 0.5−5.0% are shown in Figures S1, S3, S5, and S7 for the $J-V$ curves and EQE spectra. Device performance data are listed in Tables S1−S4. As seen here, for all these cells, the averaged PCEs of the pristine P3HT:$PC_{61}BM$ cells are 3.4−3.6%, which are comparable to the results reported in the literature,[38] ensuring that these devices are suitable for the next step: stability comparison. All these cells were then aged inside the glove box

https://dx.doi.org/10.1021/acsami.9b23366
ACS Appl. Mater. Interfaces 2020, 12, 15472−15481

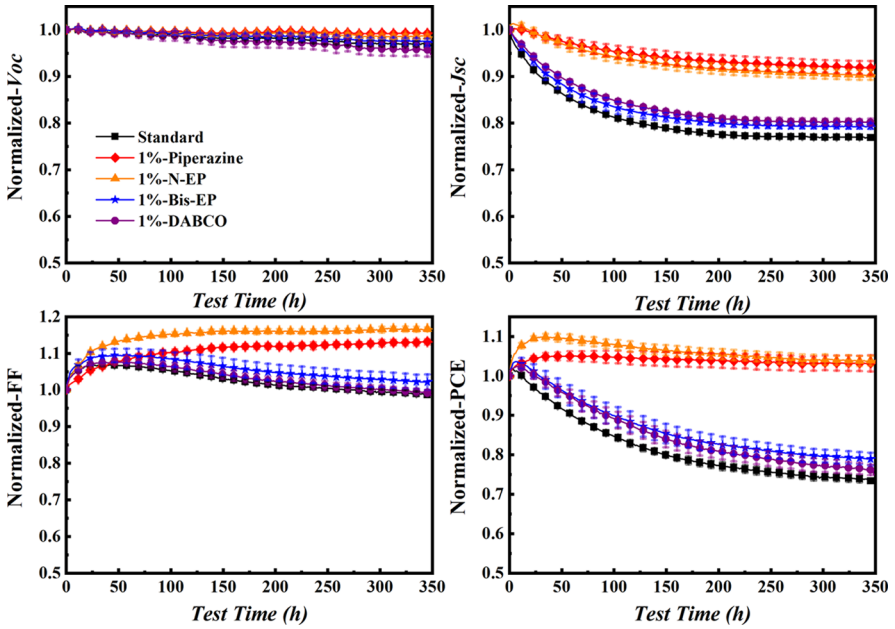

Figure 3. Degradation curves of P3HT:$PC_{61}BM$ cells doped with 1% piperazine, N-EP, Bis-EP, and DABCO under illumination.

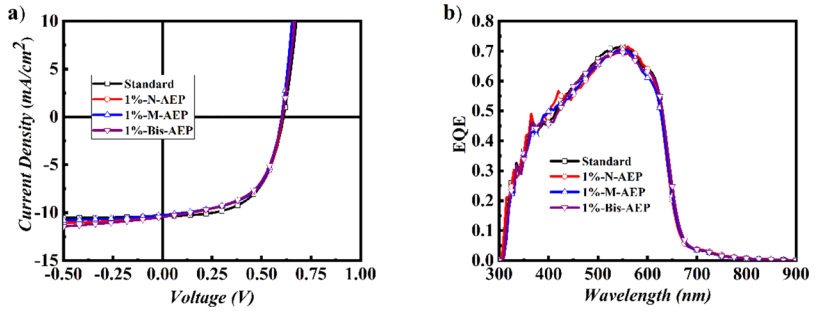

Figure 4. (a) *J*−*V* and (b) EQE curves of P3HT:$PC_{61}BM$ cells doped with 1% N-AEP, M-AEP, and Bis-AEP.

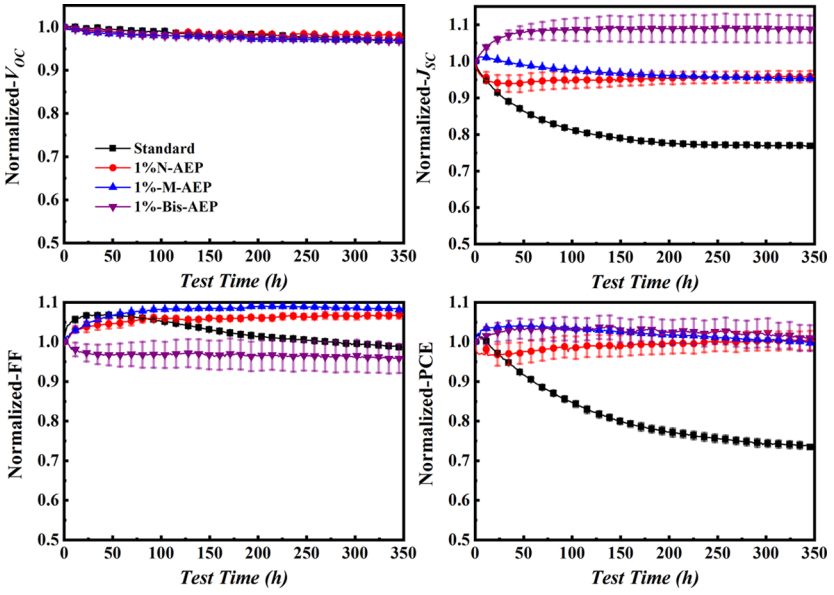

Figure 5. Degradation curves of P3HT:$PC_{61}BM$ cells with 1% N-AEP, M-AEP, and Bis-AEP.

with continuous light illumination. Figure 3 depicts the performance decay curves of these cells. The comprehensive degradation curves of the devices with other doping concentrations are shown in Figures S2, S4, S6, and S8 in the Supporting Information. As seen here, the pristine P3HT:$PC_{61}BM$ cells showed a fast burn-in performance

https://dx.doi.org/10.1021/acsami.9b23366
ACS Appl. Mater. Interfaces 2020, 12, 15472−15481

decay at the first hundred hours. The time where 80% of its initial performance (T_{80}) is reached was determined to be 148 h, and only 74% of its initial PCE remained after aging for 300 h (η_{300}/η_0). In contrast, the piperazine- and N-EP-doped cells showed slight performance improvement (η_{300}/η_0 = 103 and 104%, respectively) after aging for 300 h, clearly demonstrating the stabilization effect of piperazine and N-EP. However, the Bis-EP- and DABCO-doped cells showed almost identical decay dynamics to the pristine P3HT:$PC_{61}BM$ cells, and the T_{80} and η_{300} for these two cells were measured to be 281 and 220 h and 80 and 77%, respectively, indicating that Bis-EP and DABCO do not have any stabilizing effect. Based on these results, one can conclude that the N−H bond of piperazine plays an important role in stabilizing the device performance.

To further clarify whether only the N−H bond on the piperazine ring has the function of stabilizing the device performance, we further investigated the stabilization effect of piperazine derivatives with the 2-aminoethyl substituent, including *N*-aminoethylpiperazine (N-AEP), 1-(2-aminoethyl)-4-methylpiperazine (M-AEP), and 1,4-bis(aminoethyl)-piperazine (Bis-AEP) (see Figure1 for the chemical structures) in P3HT:$PC_{61}BM$ cells. Detailed photovoltaic performances of cells with different doping concentrations are shown in Figures S9, S11, and S13 for the *J*−*V* curves and EQE spectra and Tables S5−S7 for the photovoltaic data. The *J*−*V* and EQE curves of cells with 1% doping concentration are shown in Figure 4, and the photovoltaic performance data are also listed in Table 1. As seen here, all these aminoethyl substituted piperazine doped cells showed PCE of ∼3.5%, and no obvious device performance difference can be detected. Interestingly, all these aminoethyl-substituted piperazines can significantly improve the performance stability of the P3HT:$PC_{61}BM$ cells, as shown in Figure 5 (detailed degradation curves are shown in Figures S10, S12, and S14 in the Supporting Information), and no obvious performance decay was detected for these cells after aging for 300 h (η_{300}/η_0 values are 100−102%), clearly demonstrating the stabilizing effect of these aminoethyl-substituted piperazines. It is also worth pointing out that the stabilizing effect of these aminoethyl-substituted derivatives is mainly reflected in the stabilization of short-circuit current (J_{SC}), suggesting a similar stabilizing mechanism of piperazine derivatives.

3.2. ESR Spectra of $PC_{61}BM$:PZs Blend Films. It is known that morphology of the bicontinuous network of a bulk-heterojunction photoactive layer plays a very important role in determining the device performance.[39] It was also reported that performance of the P3HT:$PC_{61}BM$ cells is sensitive to the size of the nanocrystals of $PC_{61}BM$.[40,41] Our recent works confirmed that piperazine doping does not influence the molecular packing of P3HT and $PC_{61}BM$ within the blend film.[28] We then concluded that J_{SC} decay of the solar cells was not due to the morphology change of the photoactive layer but to the photodimerization of $PC_{61}BM$ under light illumination.[27] At the current stage, we cannot exclude the improved nanomorphology stability of the photoactive layer by piperazine doping, and suppression of dimerization of $PC_{61}BM$ was supposed to be the main reason for the stability improvement since stability improvement was mainly an effect of J_{SC}. To prove so, we first checked the light-induced electron spin resonance (LESR) of the $PC_{61}BM$:PZs blend films with different piperazine derivatives to understand the interaction of $PC_{61}BM$ and piperazine molecules under light illumination. LESR is a powerful method for probing the creation of radical species in the polymer blended films, which is related to the stability of polymer solar cells.[42−44] Our recent LESR measurement demonstrated that light-induced electron transfer between piperazine and $PC_{61}BM$ happens, leading to the formation of a $PC_{61}BM$ radical anion.[28] To correlate the stabilization effect of piperazine to the electron transfer process between PZs and $PC_{61}BM$, ESR spectra of the $PC_{61}BM$:PZs blends with or without light illumination were measured at 90 K. Figure 6 depicts the LESR spectra of these $PC_{61}BM$:PZs

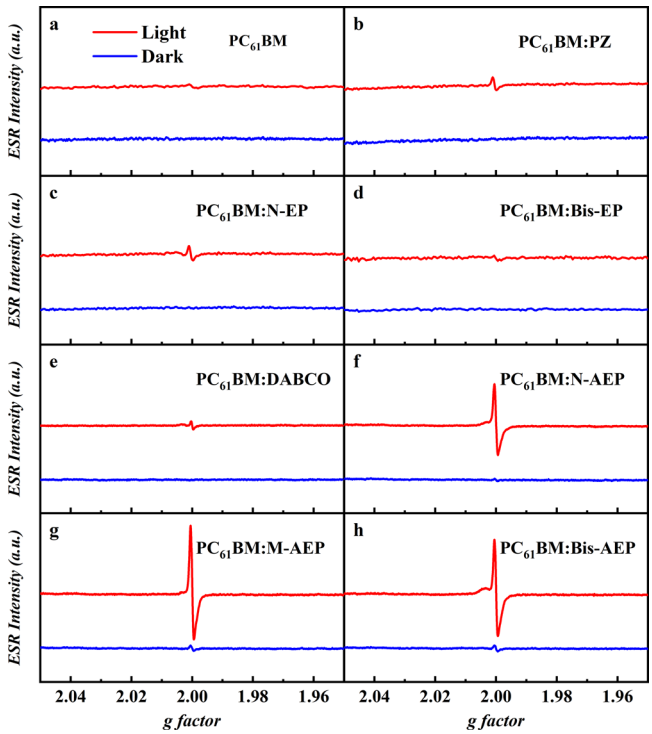

Figure 6. ESR spectra of (a) $PC_{61}BM$, (b) $PC_{61}BM$:piperazine, (c) $PC_{61}BM$:N-EP, (d) $PC_{61}BM$:Bis-EP, (e) $PC_{61}BM$:DABCO, (f) $PC_{61}BM$:N-AEP, (g) $PC_{61}BM$:M-AEP, and (h) $PC_{61}BM$:Bis-AEP blend films (1% doping concentration) measured in the dark or under light illumination at 90 K.

blend films. For the $PC_{61}BM$ net film and $PC_{61}BM$:PZs blend films, almost no signal was measured in the dark. However, when these films are illuminated with a xenon lamp, except for the $PC_{61}BM$, $PC_{61}BM$:Bis-EP, and $PC_{61}BM$:DABCO films, which showed a negligible resonance signal, all the other N−H containing piperazine doped $PC_{61}BM$ films showed a significant $PC_{61}BM$ anion signal (g = 1.9999),[45,46] confirming the photon-induced charge transfer between the N−H-containing piperazine and $PC_{61}BM$. Interestingly, the aminoethyl substituted piperazine doped films showed much intensive $PC_{61}BM$ anion signals, which could be due to the less volatility of these three compounds. The LESR results correspond very well to the stabilization effect of piperazine derivatives, where only piperazine compounds with N−H bonds show a significant stabilization effect, while the N−H-bond-free PZs showed no stabilization effect. These results confirmed that the N−H bond promotes the photon-induced electron transfer between PZs and $PC_{61}BM$.

3.3. Cyclic Voltammetry of $PC_{61}BM$ and PZs. It is known that alkylamine is able to quench the triplet of fullerene molecules through photon-induced charge transfer,[47] which is considered to be the detailed mechanism for the suppression of

https://dx.doi.org/10.1021/acsami.9b23366
ACS Appl. Mater. Interfaces 2020, 12, 15472−15481

Table 2. Oxidation and Reduction Potentials of $PC_{61}BM$ and PZs Measured by Cyclic Voltammetry and Gibbs Free Energy Calculated According to the Rehm−Weller Equation

parameter	$PC_{61}BM$	piperazine	N-EP	Bis-EP	DABCO	N-AEP	M-AEP
E_0 (V)[a]	−1.136	0.369	0.329	0.358	0.306	0.315	0.355
r^+ (Å)[b]		2.414	2.864	4.519	2.413	3.545	3.908
r^- (Å)[c]	7.666						
R_{DA} (Å)[d]		10.08	10.53	12.185	10.079	11.211	11.574
ΔG (eV)[e]		−0.153	−0.186	−0.137	−0.216	−0.191	−0.147

[a]Measured in dichloromethane at a concentration of 10^{-3} mol/L. [b]The radius of the amine cation (r^+) obtained by theoretical calculations. [c]The radius of the $PC_{61}BM$ anion (r^-) obtained by theoretical calculations. [d]$R_{DA} = (r^+) + (r^-)$. [e]Gibbs free energy calculated according to the Rehm−Weller equation (eq 1).

dimerization of $PC_{61}BM$ within the photoactive layer. The driving force for the electron transfer between piperazines and $PC_{61}BM$ can be estimated by the Rehm−Weller equation:[48,49]

$$\Delta G = e[(E(D^+/D) - E(A/A^-)] - E_T - \frac{e^2}{4\pi\varepsilon_0\varepsilon_s R_{DA}} \quad (1)$$

where ΔG is the Gibbs free energy for the electron transfer process, which indicates the possibility of electron transfer between PZs and $PC_{61}BM$; $E(D^+/D)$ and $E(A/A^-)$ are the first oxidation and reduction of the electron donor (PZs) and electron acceptor ($PC_{61}BM$), respectively, which were measured by cyclic voltammetry (CV); E_T is the triplet energy of $PC_{61}BM$ (1.5 eV);[50,51] e is the elemental electron; ε_s is the static dielectric constant of dichloromethane (DCM, ε_s = 9.03); and R_{DA} is the center-to-center distance between $PC_{61}BM$ and the amine molecule, which is estimated to be the sum of the radii of the amine cation (r^+) and $PC_{61}BM$ anion (r^-), as obtained by structure optimization of $PC_{61}BM$ and amine using DFT calculations (vide infra).

Except for Bis-AEP, which is not soluble in DCM, CVs of all other PZs were measured. Figure S15 in the Supporting Information shows the CV curves of these compounds, and the $E_0(D^+/D)$ and $E_0(A/A^-)$ data are listed in Table 2. The Gibbs free energy ΔG are then calculated according to eq 1, and the results are also listed in Table 2. As seen here, for all these PZs, ΔG is less than zero (between −0.1 and −0.2 eV), suggesting that photon-induced electron transfer from PZs to $PC_{61}BM$ is thermodynamically favorable. In addition, all these compounds have similar ΔG values, indicating that the electron transfer possibility for piperazine derivatives with different substitutions is similar for all substituted piperazines. However, experiment results (LESR and stability improvement, vide supra) indicate that only piperazine derivatives with N−H bonds show electron transfer between these two components, confirming that the N−H group plays an important role in the stabilization effect.

3.4. H^1-NMR Spectra of Piperazine with $PC_{61}BM$. The polarized N−H group of the PZs, on the other hand, makes the H atom electron-poor to be an electron acceptor, while the fullerene molecule has an electron-rich π-conjugation system. Therefore, N−H···π interaction would form when these two compounds are mixed together.[52] In addition, the carbonic ester group of $PC_{61}BM$ offers another possibility of forming N−H···O−C bonding with piperazine (H-bond). Taking into account that only piperazine compounds with N−H groups showed a stabilizing effect (vide supra) in polymer:fullerene solar cells, we speculated that the N−H···π and/or N−H···O−C bond between the piperazine and $PC_{61}BM$ is the most important factor in ensuring the stabilization effect of piperazine. To confirm the interaction between piperazine and $PC_{61}BM$ via N−H···π and/or N−H···O−C bonds, ^{1}H-NMR spectroscopy of piperazine and $PC_{61}BM$ was measured in dried benzene-d_6. Figure 7a depicts the ^{1}H-NMR spectra of

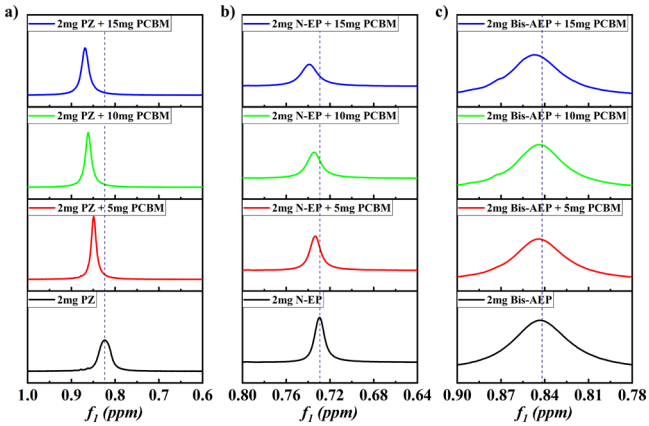

Figure 7. H^1-NMR signal of the N−H proton for (a) piperazine, (b) N-EP, (c) and Bis-AEP with the increase of $PC_{61}BM$ concentration in benzene-d_6.

piperazine with different concentrations of $PC_{61}BM$. The ^{1}H-NMR resonance peak of N−H of piperazine shifts from 0.824 to 0.869 ppm with the increase of $PC_{61}BM$ concentration. Such a downfield shift can be ascribed to the deshielding effect of the large π-conjugation system of the C_{60} core and/or the hydrogen bond between C−O and N−H. Such a phenomenon was also found for N-EP and Bis-AEP, as shown in Figure 7b,c, suggesting the existence of H-bonding between $PC_{61}BM$ and N-EP/Bis-AEP.

3.5. Intermolecular Interaction between PZs and $PC_{61}BM$. To better understand the interaction between piperazine and $PC_{61}BM$, quantum chemical calculations were performed on the piperazine-$PC_{61}BM$ adduct. Figure 8a shows

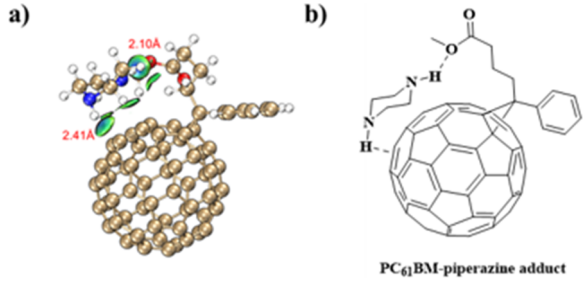

Figure 8. (a) Structure of the $PC_{61}BM$:piperazine adduct at its lowest energy state and (b) schematic sketch of this adduct.

https://dx.doi.org/10.1021/acsami.9b23366
ACS Appl. Mater. Interfaces 2020, 12, 15472−15481

the optimized structure of the $PC_{61}BM$:piperazine adduct. Independent gradient model (IGM) analysis was carried out to visualize the non-covalent interactions between the PZs and PCBM.[53] For better reading, the sketch of this adduct is shown in Figure 8b. As shown in Figure 8a, IGM analysis displays that the piperazine interacts with $PC_{61}BM$ through two major interaction areas: the one with the π aromatic system and the other with the carbonyl group on the ester side chain of PCBM. The distances between the H atom of N−H of piperazine to the closest carbon atom in the π aromatic system of $PC_{61}BM$ and the O atom of the carbonyl group are 2.41 and 2.10 Å in the optimized adduct, respectively. Such a short distance between N−H of piperazine and the $PC_{61}BM$ sphere surface infers that there exists a N−H···π hydrogen bond between them.[54,55] Also, the H···O distance of 2.10 Å is much shorter than the sum of the van der Waals radii of H (1.08 Å) and O (1.40 Å),[56] suggesting another strong hydrogen bond between piperazine and $PC_{61}BM$. Such a strong interaction was also found in $PC_{61}BM$:N-EP, $PC_{61}BM$:N-AEP, $PC_{61}BM$:M-AEP, and $PC_{61}BM$:Bis-AEP where the H···O distances are between 2.10 and 2.24 Å (see Figure S16 in the Supporting Information for the optimal structure of $PC_{61}BM$-PZs adducts and Table S8 in the Supporting Information for the calculated intermolecular distances between $PC_{61}BM$ and PZs). In contrast, for $PC_{61}BM$:Bis-EP and $PC_{61}BM$:DABCO adducts, due to the absence of the N−H group in these two piperazine compounds, there are no more hydrogen bonds formed between piperazine and PCBM.

Figure 9a,b depicts the frontier molecular orbitals (HOMO and LUMO) of $PC_{61}BM$ and $PC_{61}BM$:piperazine adduct. For

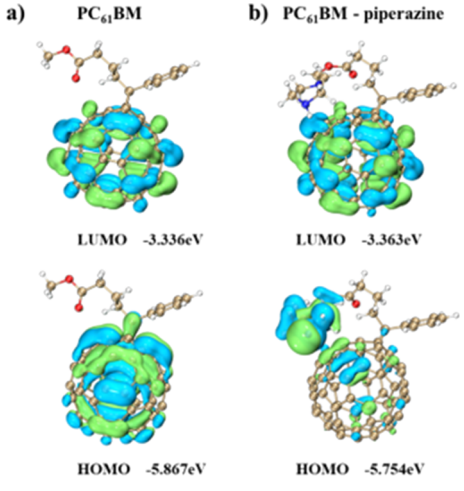

Figure 9. HOMO and LUMO of (a) $PC_{61}BM$ and (b) $PC_{61}BM$:piperazine adduct.

$PC_{61}BM$, both HOMO and LUMO are localized on the π-conjugation system of fullerene. Similar to the isolated $PC_{61}BM$, the LUMO of the $PC_{61}BM$:piperazine adduct is mainly localized in the fullerene π-moiety. However, the HOMO of the $PC_{61}BM$:piperazine adduct is found to populate on the piperazine moiety with only a small proportion on the fullerene, which can be understood by the higher electron-donating capability of piperazine. In addition, owing to the intermolecular interaction between fullerene and piperazine, the LUMO energy level decreases from −3.336 to −3.363 eV, and the HOMO energy level increases from −5.867 to −5.754 eV for $PC_{61}BM$ and the $PC_{61}BM$:piperazine adduct, respectively. In Table S9, we listed the calculated Mulliken charge values of the $PC_{61}BM$:piperazine adduct in the ground state and the lowest singlet excited state (S1). For the ground state, the overall Mulliken charge values on $PC_{61}BM$ and piperazine are calculated to be −0.06 and 0.06, respectively. When excited by light, these values turn to be −0.10 and 0.10. The different charge population between the ground and S1 excited state suggests the charge transfer from piperazine to $PC_{61}BM$, confirming the electron transfer from piperazine to $PC_{61}BM$ under light illumination.

3.6. Influence of Piperazine on Competitive Photon-Induced Electron and Energy Transfer Processes. There are two competitive processes within the P3HT:$PC_{61}BM$ blend film after light absorption by the film as shown in Figure 10: one is the photon-induced electron transfer (PET) between P3HT and $PC_{61}BM$ that leads to the formation of P3HT cations and $PC_{61}BM$ anions (process 2), which will drift to the electrodes by the built-in potential;[57] and the other one is the photon-induced energy transfer (PEnT) between P3HT and $PC_{61}BM$ that leads to the formation of the $PC_{61}BM$ singlet exciton (process 3), which will transfer to the $PC_{61}BM$ triplet through intersystem transfer (process 4).[58] The former process is the essential step for the generation of photocurrent, and higher PET efficiency generally leads to higher photocurrent. Although electron transfer between the $PC_{61}BM$ singlet and P3HT would also lead to charge separation and formation of free charge carriers, energy transfer (PEnT) efficiency between P3HT and $PC_{61}BM$ usually is very low since there is a negligible spectral overlap between the emission spectrum of P3HT and absorption spectrum of $PC_{61}BM$. This means that energy transfer processes rarely contribute to photocurrent generation in the P3HT:$PC_{61}BM$ system. However, such PEnT will form an excited singlet state of $PC_{61}BM$ (process 3), which can be further transferred to the $PC_{61}BM$ triplet through intersystem crossing (process 4) and then dimerized (process 5), causing the fast J_{SC} decay of solar cells. The PET and PEnT processes lead to the formation of $PC_{61}BM$ anions and excitons (Figure 10). Owing to the existence of H-bondings, the interaction of piperazine with $PC_{61}BM$ is much more intensive than P3HT. The energy difference for transferring P3HT excitons to $P3HT^+$ or the ground-state P3HT before and after piperazine doping can be neglected. Therefore, the energy difference for forming a $PC_{61}BM$ anion (i.e., the electron affinity energy, E_A) or $PC_{61}BM$ exciton (i.e., the exciton formation energy, E_{Ex}) upon piperazine doping can be used to assess the reaction rates of the comparative PET and PEnT processes. The calculated total energies of the different $PC_{61}BM$ species are listed in Table S10 in the Supporting Information, and the ΔE_A and ΔE_{Ex} of $PC_{61}BM$ upon piperazine doping are shown in Figure 10. As seen here, the ΔE_A for $PC_{61}BM$ after piperazine complexing was calculated to be −3.48 kcal/mol, suggesting that piperazine doping is able to promote the photon-induced electron transfer process between P3HT and $PC_{61}BM$, whereas the ΔE_{Ex} for $PC_{61}BM$ was calculated to be only −0.35 kcal/mol, suggesting that piperazine doping has a negligible influence on the photon-induced energy transfer between P3HT and $PC_{61}BM$. Overall, the calculated results confirm that piperazine doping is able to promote the photon-induced electron transfer between P3HT and $PC_{61}BM$, which is in good agreement with the enhanced device performance of the cell after piperazine doping. Moreover, intermolecular electron transfer from piperazine to $PC_{61}BM$ under excitation further inhibits triplet formation of

https://dx.doi.org/10.1021/acsami.9b23366
ACS Appl. Mater. Interfaces 2020, 12, 15472−15481

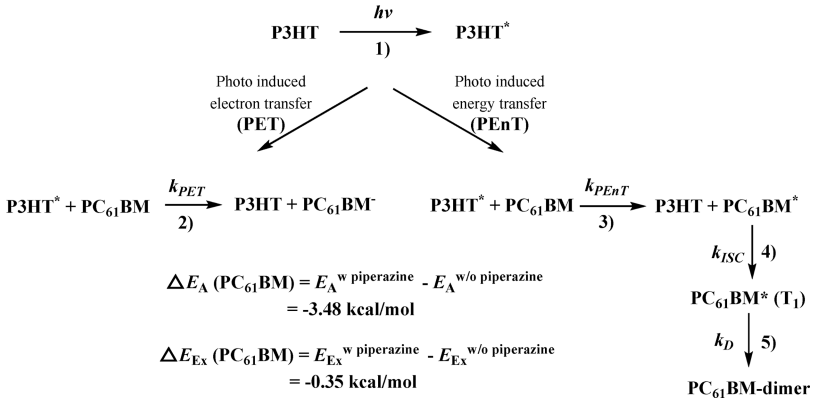

Figure 10. Processes for the photon-induced electron transfer/energy transfer between P3HT and $PC_{61}BM$.

$PC_{61}BM$, which consequently reduces the degradation processes of the P3HT:$PC_{61}BM$ cells under light illumination.

4. CONCLUSIONS

In summary, we demonstrated here that only the piperazine compounds with N−H groups are able to stabilize the performance of polymer:fullerene solar cells under light illumination. Formation of N−H···π and N−H···O−C bonds between piperazine and fullerene was confirmed by ^{1}H-NMR spectra and theoretical simulations, which bring the piperazine close to the fullerene core. Light-induced electron spin resonance (LESR) spectroscopy and theoretical simulations confirm that electron transfer (PET) between piperazine and fullerene happens when it is illuminated with light, which confirmed the quenching of $PC_{61}BM$ excitons by the piperazine derivative. In addition, since piperazine is able to stabilize the $PC_{61}BM$ anion, piperazine doping was found to be able to promote the PET process over the competitive photon-induced energy transfer (PEnT), as confirmed by the theoretical calculations. This work brings a comprehensive understanding of the stability improvement mechanism of piperazine doping in polymer solar cells, which is helpful in finding more efficient stabilizers for polymer solar cells.

■ ASSOCIATED CONTENT

Supporting Information

The Supporting Information is available free of charge at https://pubs.acs.org/doi/10.1021/acsami.9b23366.

J−*V* curves, EQE spectra, statistical data, performance, and degradation curves of polymer blend films doped with piperazine and its derivatives and calculated Mulliken charges and steady-state energies, *C*−*V* curves of PCBM and piperazine derivatives (PZs), and optimal structures of PCBM-PZs (PDF)

■ AUTHOR INFORMATION

Corresponding Authors

Hongwei Tan − *College of Chemistry, Beijing Normal University, Beijing 100875, P. R. China*; Email: hongwei.tan@bnu.edu.cn

Chang-Qi Ma − *School of Nano-Tech and Nano-Bionics, University of Science and Technology of China, Hefei 230026, P. R. China; Printable Electronics Research Center, Suzhou Institute of Nano-Tech and Nano-Bionics, Chinese Academy of Sciences, Suzhou 215123, P. R. China*; orcid.org/0000-0002-9293-5027; Email: cqma2011@sinano.ac.cn

Authors

Zerui Li − *School of Nano-Tech and Nano-Bionics, University of Science and Technology of China, Hefei 230026, P. R. China; Printable Electronics Research Center, Suzhou Institute of Nano-Tech and Nano-Bionics, Chinese Academy of Sciences, Suzhou 215123, P. R. China*

Jiankai Shan − *College of Chemistry, Beijing Normal University, Beijing 100875, P. R. China*

Lingpeng Yan − *Printable Electronics Research Center, Suzhou Institute of Nano-Tech and Nano-Bionics, Chinese Academy of Sciences, Suzhou 215123, P. R. China; Institute of New Carbon Materials, Taiyuan University of Technology, Taiyuan 030024, P. R. China*

Huimin Gu − *Printable Electronics Research Center, Suzhou Institute of Nano-Tech and Nano-Bionics, Chinese Academy of Sciences, Suzhou 215123, P. R. China; Key Laboratory of Interface Science and Engineering in Advanced Materials, Ministry of Education, Taiyuan University of Technology, Taiyuan 030024, P. R. China*

Yi Lin − *Department of Chemistry, Xi'an Jiaotong Liverpool University, Suzhou 215123, P. R. China*

Complete contact information is available at: https://pubs.acs.org/10.1021/acsami.9b23366

Notes

The authors declare no competing financial interest.

■ ACKNOWLEDGMENTS

The authors would like to acknowledge the financial support from the Ministry of Science and Technology of China (No. 2016YFA0200700), the National Natural Science Foundation of China (61904121 and 21571019), Chinese Academy of Sciences (No. YJKYYQ20180029 and CAS-ITRI 2019010), and Youth Innovation Promotion Association, CAS (2019317).

■ REFERENCES

(1) Sun, C.; Pan, F.; Bin, H.; Zhang, J.; Xue, L.; Qiu, B.; Wei, Z.; Zhang, Z.-G.; Li, Y. A Low Cost and High Performance Polymer Donor Material for Polymer Solar Cells. *Nat. Commun.* **2018**, *9*, 743.

(2) Jinno, H.; Fukuda, K.; Xu, X.; Park, S.; Suzuki, Y.; Koizumi, M.; Yokota, T.; Osaka, I.; Takimiya, K.; Someya, T. Stretchable and Waterproof Elastomer-Coated Organic Photovoltaics for Washable Electronic Textile Applications. *Nat. Energy* **2017**, *2*, 780−785.

(3) Han, Y.; Chen, X.; Wei, J.; Ji, G.; Wang, C.; Zhao, W.; Lai, J.; Zha, W.; Li, Z.; Yan, L.; Gu, H.; Luo, Q.; Chen, Q.; Chen, L.; Hou, J.; Su, W.; Ma, C.-Q. Efficiency above 12% for 1 cm^2Flexible Organic

Solar Cells with Ag/Cu Grid Transparent Conducting Electrode. *Adv. Sci.* **2019**, 1901490.
(4) Kaltenbrunner, M.; White, M. S.; Głowacki, E. D.; Sekitani, T.; Someya, T.; Sariciftci, N. S.; Bauer, S. Ultrathin and Lightweight Organic Solar Cells with High Flexibility. *Nat. Commun.* **2012**, *3*, 770.
(5) Dong, S.; Zhang, K.; Xie, B.; Xiao, J.; Yip, H.-L.; Yan, H.; Huang, F.; Cao, Y. High-Performance Large-Area Organic Solar Cells Enabled by Sequential Bilayer Processing via Nonhalogenated Solvents. *Adv. Energy Mater.* **2019**, *9*, 1802832.
(6) Xue, R.; Zhang, J.; Li, Y.; Li, Y. Organic Solar Cell Materials toward Commercialization. *Small* **2018**, *14*, 1801793.
(7) Cui, Y.; Yao, H.; Zhang, J.; Zhang, T.; Wang, Y.; Hong, L.; Xian, K.; Xu, B.; Zhang, S.; Peng, J.; Wei, Z.; Gao, F.; Hou, J. Over 16% Efficiency Organic Photovoltaic Cells Enabled by a Chlorinated Acceptor with Increased Open-Circuit Voltages. *Nat. Commun.* **2019**, *10*, 2515.
(8) Fan, B.; Zhang, D.; Li, M.; Zhong, W.; Zeng, Z.; Ying, L.; Huang, F.; Cao, Y. Achieving over 16% Efficiency for Single-Junction Organic Solar Cells. *Sci. China Chem.* **2019**, *62*, 746−752.
(9) Meng, L.; Zhang, Y.; Wan, X.; Li, C.; Zhang, X.; Wang, Y.; Ke, X.; Xiao, Z.; Ding, L.; Xia, R.; Yip, H.-L.; Cao, Y.; Chen, Y. Organic and Solution-Processed Tandem Solar Cells with 17.3% Efficiency. *Science* **2018**, *361*, 1094−1098.
(10) Cheng, P.; Zhan, X. Stability of Organic Solar Cells: Challenges and Strategies. *Chem. Soc. Rev.* **2016**, *45*, 2544−2582.
(11) Kang, H.; Kim, G.; Kim, J.; Kwon, S.; Kim, H.; Lee, K. Bulk-Heterojunction Organic Solar Cells: Five Core Technologies for Their Commercialization. *Adv. Mater.* **2016**, *28*, 7821−7861.
(12) Jeong, J.; Seo, J.; Nam, S.; Han, H.; Kim, H.; Anthopoulos, T. D.; Bradley, D. D. C.; Kim, Y. Significant Stability Enhancement in High-Efficiency Polymer:Fullerene Bulk Heterojunction Solar Cells by Blocking Ultraviolet Photons from Solar Light. *Adv. Sci.* **2016**, *3*, 1500269.
(13) Lee, H. K. H.; Telford, A. M.; Röhr, J. A.; Wyatt, M. F.; Rice, B.; Wu, J.; de Castro Maciel, A.; Tuladhar, S. M.; Speller, E.; McGettrick, J.; Searle, J. R.; Pont, S.; Watson, T.; Kirchartz, T.; Durrant, J. R.; Tsoi, W. C.; Nelson, J.; Li, Z. The Role of Fullerenes in the Environmental Stability of Polymer:Fullerene Solar Cells. *Energy Environ. Sci.* **2018**, *11*, 417−428.
(14) Yang, D.; Löhrer, F. C.; Körstgens, V.; Schreiber, A.; Bernstorff, S.; Buriak, J. M.; Müller-Buschbaum, P. In-Operando Study of the Effects of Solvent Additives on the Stability of Organic Solar Cells Based on PTB7-Th:PC71BM. *ACS Energy Lett.* **2019**, *4*, 464−470.
(15) Perthué, A.; Gorisse, T.; Silva, H. S.; Lombard, C.; Bégué, D.; Hudhomme, P.; Pépin-Donat, B.; Rivaton, A.; Wantz, G. New Insights into Polymer Solar Cells Stability: The Crucial Role of PCBM Oxidation. *J. Mater. Res.* **2018**, *33*, 1868−1878.
(16) Kim, J. B.; Kim, C. S.; Kim, Y. S.; Loo, Y. L. Oxidation of Silver Electrodes Induces Transition from Conventional to Inverted Photovoltaic Characteristics in Polymer Solar Cells. *Appl. Phys. Lett.* **2009**, *95*, 183301.
(17) Shin, M.; Kim, H.; Park, J.; Nam, S.; Heo, K.; Ree, M.; Ha, C. S.; Kim, Y. Abrupt Morphology Change upon Thermal Annealing in Poly(3-Hexylthiophene)/Soluble Fullerene Blend Films for Polymer Solar Cells. *Adv. Funct. Mater.* **2010**, *20*, 748−754.
(18) Zhou, W.; Shi, J.; Lv, L.; Chen, L.; Chen, Y. A Mechanistic Investigation of Morphology Evolution in P3HT-PCBM Films Induced by Liquid Crystalline Molecules under External Electric Field. *Phys. Chem. Chem. Phys.* **2015**, *17*, 387−397.
(19) Mateker, W. R.; McGehee, M. D. Progress in Understanding Degradation Mechanisms and Improving Stability in Organic Photovoltaics. *Adv. Mater.* **2017**, *29*, 1603940.
(20) Heumueller, T.; Mateker, W. R.; Distler, A.; Fritze, U. F.; Cheacharoen, R.; Nguyen, W. H.; Biele, M.; Salvador, M.; von Delius, M.; Egelhaaf, H.-J.; McGehee, M. D.; Brabec, C. J. Morphological and Electrical Control of Fullerene Dimerization Determines Organic Photovoltaic Stability. *Energy Environ. Sci.* **2016**, *9*, 247−256.
(21) González, D. M.; Körstgens, V.; Yao, Y.; Song, L.; Santoro, G.; Roth, S. V.; Müller-Buschbaum, P. Improved Power Conversion Efficiency of P3HT:PCBM Organic Solar Cells by Strong Spin-Orbit Coupling-Induced Delayed Fluorescence. *Adv. Energy Mater.* **2015**, *5*, 1401770.
(22) Gevorgyan, S. A.; Espinosa, N.; Ciammaruchi, L.; Roth, B.; Livi, F.; Tsopanidis, S.; Züfle, S.; Queirós, S.; Gregori, A.; Benatto, G. A. D. R.; Corazza, M.; Madsen, M. V.; Hösel, M.; Beliatis, M. J.; Larsen-Olsen, T. T.; Pastorelli, F.; Castro, A.; Mingorance, A.; Lenzi, V.; Fluhr, D.; Roesch, R.; Ramos, M. M. D.; Savva, A.; Hoppe, H.; Marques, L. S. A.; Burgués, I.; Georgiou, E.; Serrano-Luján, L.; Krebs, F. C. Baselines for Lifetime of Organic Solar Cells. *Adv. Energy Mater.* **2016**, *6*, 1600910.
(23) Turkovic, V.; Engmann, S.; Tsierkezos, N.; Hoppe, H.; Ritter, U.; Gobsch, G. Long-Term Stabilization of Organic Solar Cells Using Hindered Phenols as Additives. *ACS Appl. Mater. Interfaces* **2014**, *6*, 18525−18537.
(24) Turkovic, V.; Prete, M.; Bregnhøj, M.; Inasaridze, L.; Volyniuk, D.; Obrezkov, F. A.; Grazulevicius, J. V.; Engmann, S.; Rubahn, H.-G.; Troshin, P. A.; Ogilby, P. R.; Madsen, M. Biomimetic Approach to Inhibition of Photooxidation in Organic Solar Cells Using Beta-Carotene as an Additive. *ACS Appl. Mater. Interfaces* **2019**, *11*, 41570−41579.
(25) Salvador, M.; Gasparini, N.; Perea, J. D.; Paleti, S. H.; Distler, A.; Inasaridze, L. N.; Troshin, P. A.; Lüer, L.; Egelhaaf, H.-J.; Brabec, C. Suppressing Photooxidation of Conjugated Polymers and Their Blends with Fullerenes Through Nickel Chelates. *Energy Environ. Sci.* **2017**, *10*, 2005−2016.
(26) Distler, A.; Sauermann, T.; Egelhaaf, H. J.; Rodman, S.; Waller, D.; Cheon, K. S.; Lee, M.; Guldi, D. M. The Effect of PCBM Dimerization on the Performance of Bulk Heterojunction Solar Cells. *Adv. Energy Mater.* **2014**, *4*, 1300693.
(27) Yan, L.; Yi, J.; Chen, Q.; Dou, J.; Yang, Y.; Liu, X.; Chen, L.; Ma, C.-Q. External Load-Dependent Degradation of P3HT:PC61BM Solar Cells: Behavior, Mechanism, and Method of Suppression. *J. Mater. Chem. A* **2017**, *5*, 10010−10020.
(28) Yan, L.; Wang, Y.; Wei, J.; Ji, G.; Gu, H.; Li, Z.; Zhang, J.; Luo, Q.; Wang, Z.; Liu, X.; Xu, B.; Wei, Z.; Ma, C.-Q. Simultaneous Performance and Stability Improvement of Polymer:Fullerene Solar Cells by Doping with Piperazine. *J. Mater. Chem. A* **2019**, *7*, 7099−7108.
(29) Zhang, C.; Heumueller, T.; Leon, S.; Gruber, W.; Burlafinger, K.; Tang, X.; Perea, J. D.; Wabra, I.; Hirsch, A.; Unruh, T.; Li, N.; Brabec, C. J. A Top-Down Strategy Identifying Molecular Phase Stabilizers to Overcome Microstructure Instabilities in Organic Solar Cells. *Energy Environ. Sci.* **2019**, *12*, 1078−1087.
(30) Beek, W. J. E.; Wienk, M. M.; Kemerink, M.; Yang, X.; Janssen, R. A. J. Hybrid Zinc Oxide Conjugated Polymer Bulk Heterojunction Solar Cells. *J. Phys. Chem. B* **2005**, *109*, 9505−9516.
(31) Frisch, M. J.; Trucks, G. W.; Schlegel, H. B.; Scuseria, G. E.; Robb, M. A.; Cheeseman, J. R.; Scalmani, G.; Barone, V.; Petersson, G. A.; Nakatsuji, H.; Li, X.; Caricato, M.; Marenich, A. V.; Bloino, J.; Janesko, B. G.; Gomperts, R.; Mennucci, B.; Hratchian, H. P.; Ortiz, J. V.; Izmaylov, A. F.; Sonnenberg, J. L.; Williams; Ding, F.; Lipparini, F.; Egidi, F.; Goings, J.; Peng, B.; Petrone, A.; Henderson, T.; Ranasinghe, D.; Zakrzewski, V. G.; Gao, J.; Rega, N.; Zheng, G.; Liang, W.; Hada, M.; Ehara, M.; Toyota, K.; Fukuda, R.; Hasegawa, J.; Ishida, M.; Nakajima, T.; Honda, Y.; Kitao, O.; Nakai, H.; Vreven, T.; Throssell, K.; Montgomery, Jr., J. A.; Peralta, J. E.; Ogliaro, F.; Bearpark, M. J.; Heyd, J. J.; Brothers, E. N.; Kudin, K. N.; Staroverov, V. N.; Keith, T. A.; Kobayashi, R.; Normand, J.; Raghavachari, K.; Rendell, A. P.; Burant, J. C.; Iyengar, S. S.; Tomasi, J.; Cossi, M.; Millam, J. M.; Klene, M.; Adamo, C.; Cammi, R.; Ochterski, J. W.; Martin, R. L.; Morokuma, K.; Farkas, O.; Foresman, J. B.; Fox, D. J. *Gaussian 09 Rev. D.01*; Gaussian: Wallingford, CT, 2013.
(32) Weigend, F.; Ahlrichs, R. Balanced Basis Sets of Split Valence, Triple Zeta Valence and Quadruple Zeta Valence Quality for H To Rn: Design and Assessment of Accuracy. *Phys. Chem. Chem. Phys.* **2005**, *7*, 3297−3305.
(33) Stephens, P. J.; Devlin, F. J.; Chabalowski, C. F.; Frisch, M. J. Ab Initio Calculation of Vibrational Absorption and Circular

https://dx.doi.org/10.1021/acsami.9b23366
ACS Appl. Mater. Interfaces 2020, 12, 15472−15481

Dichroism Spectra Using Density-Functional Force Fields. *J. Phys. Chem.* **1994**, *98*, 11623−11627.
(34) Grimme, S.; Ehrlich, S.; Goerigk, L. Effect of the Damping Function in Dispersion Corrected Density Functional Theory. *J. Comput. Chem.* **2011**, *32*, 1456−1465.
(35) Boys, S. F.; Bernardi, F. The Calculation of Small Molecular Interactions by The Differences of Separate Total Energies. Some Procedures with Reduced Errors. *Mol. Phys.* **2002**, *100*, 65−73.
(36) Simon, S.; Duran, M.; Dannenberg, J. J. How does Basis Set Superposition Error Change The Potential Surfaces for Hydrogen Bonded Dimers? *J. Chem. Phys.* **1996**, *105*, 11024−11031.
(37) Lu, T.; Chen, F. Multiwfn: A Multifunctional Wavefunction Analyzer. *J. Comput. Chem.* **2012**, *33*, 580−592.
(38) Dang, M. T.; Hirsch, L.; Wantz, G. P3HT:PCBM, Best Seller in Polymer Photovoltaic Research. *Adv. Mater.* **2011**, *23*, 3597−3602.
(39) Zhao, F.; Wang, C.; Zhan, X. Morphology Control in Organic Solar Cells. *Adv. Energy Mater.* **2018**, *8*, 1703147.
(40) Liao, H. C.; Tsao, C. S.; Lin, T. H.; Chuang, C. M.; Chen, C. Y.; Jeng, U. S.; Su, C. H.; Chen, Y. F.; Su, W. F. Quantitative Nanoorganized Structural Evolution for a High Efficiency Bulk Heterojunction Polymer Solar Cell. *J. Am. Chem. Soc.* **2011**, *133*, 13064−13073.
(41) Liao, H. C.; Tsao, C. S.; Lin, T. H.; Jao, M. H.; Chuang, C. M.; Chang, S. Y.; Huang, Y. C.; Shao, Y. T.; Chen, C. Y.; Su, C. J.; Jeng, U. S.; Chen, Y. F.; Su, W. F. Nanoparticle-Tuned Self-Organization of a Bulk Heterojunction Hybrid Solar Cell with Enhanced Performance. *ACS Nano* **2012**, *6*, 1657−1666.
(42) Inasaridze, L. N.; Shames, A. I.; Martynov, I. V.; Li, B.; Mumyatov, A. V.; Susarova, D. K.; Katz, E. A.; Troshin, P. A. Light-Induced Generation of Free Radicals by Fullerene Derivatives: An Important Degradation Pathway in Organic Photovoltaics? *J. Mater. Chem. A* **2017**, *5*, 8044−8050.
(43) Frolova, L. A.; Piven, N. P.; Susarova, D. K.; Akkuratov, A. V.; Babenko, S. D.; Troshin, P. A. ESR Spectroscopy for Monitoring the Photochemical and Thermal Degradation of Conjugated Polymers Used as Electron Donor Materials in Organic Bulk Heterojunction Solar Cells. *Chem. Commun.* **2015**, *51*, 2242−2244.
(44) Susarova, D. K.; Piven, N. P.; Akkuratov, A. V.; Frolova, L. A.; Polinskaya, M. S.; Ponomarenko, S. A.; Babenko, S. D.; Troshin, P. A. ESR Spectroscopy as a Powerful Tool for Probing the Quality of Conjugated Polymers Designed for Photovoltaic Applications. *Chem. Commun.* **2015**, *51*, 2239−2241.
(45) Havlicek, M.; Sariciftci, N. S.; Scharber, M. C. Degradation Kinetics in Different Polymer-Fullerene Blends Investigated by Electron Spin Resonance. *J. Mater. Res.* **2018**, *33*, 1853−1859.
(46) Aguirre, A.; Meskers, S. C. J.; Janssen, R. A. J.; Egelhaaf, H. J. Formation of Metastable Charges as a First Step in Photoinduced Degradation in π-Conjugated Polymer: Fullerene Blends for Photovoltaic Applications. *Org. Electron.* **2011**, *12*, 1657−1662.
(47) Arbogast, J. W.; Foote, C. S.; Kao, M. Electron Transfer to Triplet fullerene C60. *J. Am. Chem. Soc.* **1992**, *114*, 2277−2279.
(48) Oevering, H.; Paddon-Row, M. N.; Heppener, M.; Oliver, A. M.; Cotsaris, E.; Verhoeven, J. W.; Hush, N. S. Long-Range Photoinduced through-Bond Electron-Transfer and Radiative Recombination Via Rigid Nonconjugated Bridges - Distance and Solvent Dependence. *J. Am. Chem. Soc.* **1987**, *109*, 3258−3269.
(49) Prasad, E.; Gopidas, K. R. Photoinduced Electron Transfer in Hydrogen Bonded Donor-Acceptor Systems. Study of the Dependence of Rate on Free Energy and Simultaneous Observation of the Marcus and Rehm-Weller Behaviors. *J. Am. Chem. Soc.* **2000**, *122*, 3191−3196.
(50) Chow, P. C. Y.; Albert-Seifried, S.; Gélinas, S.; Friend, R. H. Nanosecond Intersystem Crossing Times in Fullerene Acceptors: Implications for Organic Photovoltaic Diodes. *Adv. Mater.* **2014**, *26*, 4851−4854.
(51) Di Nuzzo, D.; Aguirre, A.; Shahid, M.; Gevaerts, V. S.; Meskers, S. C. J.; Janssen, R. A. J. Improved Film Morphology Reduces Charge Carrier Recombination into the Triplet Excited State in a Small Bandgap Polymer-Fullerene Photovoltaic Cell. *Adv. Mater.* **2010**, *22*, 4321−4324.
(52) Keiluweit, M.; Kleber, M. Molecular-Level Interactions in Soils and Sediments: The Role of Aromatic pi-Systems. *Environ. Sci. Technol.* **2009**, *43*, 3421−3429.
(53) Lefebvre, C.; Rubez, G.; Khartabil, H.; Boisson, J.-C.; Contreras-García, J.; Hénon, E. Accurately Extracting the Signature of Intermolecular Interactions Present in the NCI Plot of the Reduced Density Gradient Versus Electron Density. *Phys. Chem. Chem. Phys.* **2017**, *19*, 17928−17936.
(54) Tsuzuki, S.; Honda, K.; Uchimaru, T.; Mikami, M.; Tanabe, K. Origin of the Attraction and Directionality of the NH/π Interaction: Comparison with OH/π and CH/π Interactions. *J. Am. Chem. Soc.* **2000**, *122*, 11450−11458.
(55) Mohan, N.; Vijayalakshmi, K. P.; Koga, N.; Suresh, C. H. Comparison of Aromatic NH···π, OH···π, and CH···π Interactions of Alanine Using MP2, CCSD, and DFT Methods. *J. Comput. Chem.* **2010**, *31*, 2874−2882.
(56) Hu, S. Z.; Zhou, Z. H.; Tsai, K. R. Average Van der Waals Radii of Atoms in CrystaIs. *Acta Phys.-Chim. Sin.* **2003**, *19*, 1073−1077.
(57) Lukina, E. A.; Popov, A. A.; Uvarov, M. N.; Kulik, L. V. Out-of-Phase Electron Spin Echo Studies of Light-Induced Charge-Transfer States in P3HT/PCBM Composite. *J. Phys. Chem. B* **2015**, *119*, 13543−13548.
(58) Wang, J.; Enevold, J.; Edman, L. Photochemical Transformation of Fullerenes. *Adv. Funct. Mater.* **2013**, *23*, 3220−3225.

https://dx.doi.org/10.1021/acsami.9b23366
ACS Appl. Mater. Interfaces 2020, 12, 15472−15481